Changes in dose with segmentation of breast tissues in Monte Carlo calculations for low-energy brachytherapy

J. G. H. Sutherland,[a] R. M. Thomson, and D. W. O. Rogers
Carleton Laboratory for Radiotherapy Physics, Department of Physics, Carleton University, Ottawa K1S 5B6, Canada

(Received 26 April 2011; revised 27 June 2011; accepted for publication 29 June 2011; published 1 August 2011)

Purpose: To investigate the use of various breast tissue segmentation models in Monte Carlo dose calculations for low-energy brachytherapy.
Methods: The EGSnrc user-code BrachyDose is used to perform Monte Carlo simulations of a breast brachytherapy treatment using TheraSeed Pd-103 seeds with various breast tissue segmentation models. Models used include a phantom where voxels are randomly assigned to be gland or adipose (randomly segmented), a phantom where a single tissue of averaged gland and adipose is present (averaged tissue), and a realistically segmented phantom created from previously published numerical phantoms. Radiation transport in averaged tissue while scoring in gland along with other combinations is investigated. The inclusion of calcifications in the breast is also studied in averaged tissue and randomly segmented phantoms.
Results: In randomly segmented and averaged tissue phantoms, the photon energy fluence is approximately the same; however, differences occur in the dose volume histograms (DVHs) as a result of scoring in the different tissues (gland and adipose versus averaged tissue), whose mass energy absorption coefficients differ by 30%. A realistically segmented phantom is shown to significantly change the photon energy fluence compared to that in averaged tissue or randomly segmented phantoms. Despite this, resulting DVHs for the entire treatment volume agree reasonably because fluence differences are compensated by dose scoring differences. DVHs for the dose to only the gland voxels in a realistically segmented phantom do not agree with those for dose to gland in an averaged tissue phantom. Calcifications affect photon energy fluence to such a degree that the differences in fluence are not compensated for (as they are in the no calcification case) by dose scoring in averaged tissue phantoms.
Conclusions: For low-energy brachytherapy, if photon transport and dose scoring both occur in an averaged tissue, the resulting DVH for the entire treatment volume is reasonably accurate because inaccuracies in photon energy fluence are compensated for by inaccuracies in localized dose scoring. If dose to fibroglandular tissue in the breast is of interest, then the inaccurate photon energy fluence calculated in an averaged tissue phantom will result in inaccurate DVHs and average doses for those tissues. Including calcifications necessitates the use of proper tissue segmentation. © *2011 American Association of Physicists in Medicine*. [DOI: 10.1118/1.3613167]

Key words: brachytherapy dose calculations, tissue segmentation, Monte Carlo, EGSnrc, Pd-103, breast cancer

I. INTRODUCTION

Historically, dose in a homogeneous, water environment has been the primary focus of brachytherapy dosimetry, as seen in the TG-43 (Ref. 1) protocol. One of the advantages of Monte Carlo dose calculations is the possibility of modeling segmented, nonwater media in simulations. The use of more detailed models raises important issues such as the level of detail needed to accurately compute the dose, the choice of tissues and media to include, as well as the required accuracy of the compositions. Further, there is the question of which tissues are of clinical interest. As the brachytherapy community considers clinical implementation and possible future adoption of model-based dose calculation algorithms, these considerations are of increasing importance.

These issues arise when considering nonwater breast models for Monte Carlo calculations. Breast tissue generally consists of fibroglandular and adipose tissues, possibly with some calcifications. The proportion of each of these tissues in a typical breast has been studied by Yaffe *et al.*,[2] who found that the mean percentage of fibroglandular tissue was 19.3% by volume. The dose to fibroglandular tissue is the quantity of interest in mammography radiation protection[2–5] and may also be relevant for brachytherapy treatments as the linear attenuation coefficients of gland and tumour are similar.[6,7] With the advent of ^{103}Pd treatments, the use of 50 kV electronic brachytherapy sources for partial breast irradiation and the use of model-based dose calculation algorithms, there is increasing interest in the role of breast tissue composition in brachytherapy.[8–10]

Current model-based practices in Monte Carlo simulations for brachytherapy typically use homogeneous averaged tissues to represent different ratios of glandular and adipose

tissue.[8,10] Sometimes, CT data are used to assign the mass density to each voxel.[8] Photon transport and energy deposition are modeled in these averaged tissues. While more recent work has begun to investigate breast tissue segmentation[11] and the importance of tissue segmentation for kilovoltage beams,[12] the differences between the dose to the separate glandular and adipose tissues have been largely ignored in treatment planning studies.

In mammography radiation protection, it is common to estimate the average dose to the glandular tissue[2–5] by transporting photons through an averaged tissue and then calculating the portion of energy deposited in the fibroglandular tissue using ratios of mass energy absorption coefficients. In effect, photon transport is modeled in the averaged tissue and energy deposition to gland is calculated.

The question of the accuracy of using homogeneous averaged tissues in breast calculations and under which conditions their use might be justified in lieu of fully segmented phantoms has not yet been thoroughly investigated. The purpose of this work is to investigate the effects of more realistic segmentation of breast tissues in model-based Monte Carlo breast dosimetry. Possible inaccuracies may occur during the transport of particles through the breast creating differences in the photon energy fluence, and during the deposition of dose because of choices of dose scoring media and incorrect photon energy fluence. In this paper, the current model-based practices of brachytherapy and mammography radiation protection are investigated and compared to fully segmented calculations. The modeling of calcifications in the breast is also investigated.

II. METHODS

Monte Carlo calculations are performed with the EGSnrc[13] user-code BrachyDose.[14,15] BrachyDose estimates dose as collision kerma scored with a tracklength estimator using mass energy absorption coefficients (calculated with the EGSnrc user-code g). In all calculations, 64 fully modeled[16] TheraSeed 200 ^{103}Pd brachytherapy seeds [mean emerging photon energy of 20.71 keV (Ref. 17)] are placed in a cube formation centered around the center of the phantom, (0,0,0) cm, with central x, y, and z coordinates of ± 1.55 cm or ± 0.55 cm and axes parallel to the z-axis. The 0.05 cm offsets ensure that the centers of the seeds do not lie on voxel boundaries. A 64 cm^3 planning treatment volume (PTV) region is defined as a cube ranging from (2,2,2) cm to (−2,−2,−2) cm. As these dimensions represent a larger PTV and lower seed density than the median clinical dimensions,[18] calculations are also performed with seed central x, y, and z coordinates of ± 0.92 cm or ± 0.46 cm with a PTV ranging from (1.23,1.23,1.23) cm to (−1.23,−1.23,−1.23) cm to approximate a clinically small dense treatment.

For voxels containing seeds, doses are calculated by employing a volume correction to account for the volume occupied by the seeds. Simulations of 10^9 histories achieve statistical uncertainties of less than 0.2% on the dose in voxels in the PTV. These high precision calculations are not necessarily needed for the calculation of dose volume histograms (DVHs) as simulations of 10^7 histories produce nearly indistinguishable curves.

Densities and elemental compositions of breast tissues and breast calcifications are taken from Woodard and White 1986 (Ref. 19) and ICRU Report 46 (Ref. 20), respectively, (Table I). The averaged breast tissues in this work are specified as percent mixtures by mass. For most calculations, proportions of 25% fibroglandular tissue and 75% adipose tissue by mass (23.7% and 76.3% by volume) are used to approximate the recommendations of Yaffe *et al.*[2] The mass energy absorption coefficient ratios of fibroglandular tissue, adipose tissue, and a 25% gland 75% adipose mixture (by mass) to water are within a range of ± 0.01 over the photon energy range of 10–30 keV, at 0.80 (gland/water), 0.60 (adipose/water), and 0.65 ((25/75 mixture)/water), respectively.

Physical dose distributions and dose volume histograms are both calculated. To investigate the doses to adipose and fibroglandular tissues separately, an in-house code was developed to allow the calculation of DVHs, wherein the volume considered consists only of those voxels within the PTV containing one medium (e.g., DVHs for voxels containing gland only).

II.A. Dose to gland and adipose versus dose to an averaged tissue

For this portion of the study, a simple geometry configuration defined as a $12 \times 12 \times 12$ cm^3 phantom with (1 mm)^3 voxels is used to approximate a breast brachytherapy treatment; dose distributions are unchanged within statistics with (2 mm)^3 voxels. The PTV is at the center of the phantom. The whole phantom is filled with an averaged tissue of given proportions of gland and adipose or each voxel is randomly assigned a single tissue so as to create a phantom with the same proportion of tissues by mass. For example, one phantom has voxels containing a single averaged tissue (25% gland and 75% adipose by mass), while the other has each voxel randomly assigned gland or adipose so as to maintain this proportion by mass over the entire phantom. These phantoms are called "25/75-averaged-tissue phantom" and "25/75-randomly-segmented phantom," respectively, and the averaged tissue is denoted by 25/75-averaged-tissue. In general, the naming scheme used in this work is *[proportions of gland/adipose(/calcification) by mass]-[segmentation model]*. For the averaged tissue phantoms, dose is scored either in the averaged tissue (to investigate the method often

TABLE I. Composition of breast tissues. Densities and elemental compositions of breast tissues and breast calcifications were taken from Woodard and White 1986 (Ref. 19) and ICRU report 46 (Ref. 20), respectively.

	Composition (Mass %)									
Material	H	C	N	O	Na	P	S	Cl	Ca	Density (g/cm^3)
Fibroglandular	10.6	33.2	3.0	52.7	0.1	0.1	0.2	0.1	0.0	1.02
Adipose	11.4	59.8	0.7	27.8	0.1	0.0	0.1	0.1	0.0	0.95
Calcification	0.3	1.6	0.5	40.7	0.0	18.7	0.0	0.0	38.2	3.06

used in brachytherapy calculations) or in fibroglandular tissue (to investigate the method used for mammography radiation protection studies[2–4] albeit with a much different source geometry). For randomly segmented phantoms, dose is scored in the tissue of each particular voxel.

These phantoms are used to investigate the hypothesis that the photon energy fluence remains relatively unchanged between an averaged tissue phantom and a randomly segmented phantom. Assuming this is the case, these phantoms can provide information concerning dose differences that arise from modeling gland and adipose tissues separately or using an averaged tissue phantom independent of the effects of differing photon energy fluence. Figures 1(a) and 1(b) show representational slices of the 25/75-averaged-tissue and 25/75-randomly-segmented phantoms, respectively.

II.B. Effect of realistic segmentation on photon energy fluence

To approximate a realistically segmented breast, a phantom was created using a numerical breast phantom from the work of Zastrow *et al.*[21] Breast phantom 070604PA1 was chosen, because its proportions are nearly 25% gland and 75% adipose by mass. This phantom contains three classes of fibroglandular and adipose tissues that differ in their dielectric properties. Voxels in the Zastrow phantom containing any class of fibroglandular (adipose) tissue are set to the fibroglandular (adipose) tissue (composition found in Table I) in the phantoms for the present work. The numerical phantom also contains a so-called transitional tissue (having dielectric properties transitioning between gland and adipose), which is approximated in the phantoms for the present work as being 50% adipose and 50% fibroglandular tissues by mass. The center of the phantom for the present work is set to (0,0,0) cm and a $5 \times 5 \times 5$ cm^3 centered cube of $0.5 \times 0.5 \times 0.5$ mm^3 voxels is taken from the numerical phantom of voxels of the same size. The $5 \times 5 \times 5$ cm^3 detailed cube is surrounded by single, large voxels of adipose tissue that extend to the outer dimensions of the numerical phantom ($x = \pm 7.5$ cm, $y = \pm 9.55$ cm, and $z = \pm 6.75$ cm). In the detailed cube, 9% of voxels are gland, 31% are 50/50 gland/adipose, and 60% are adipose [see a typical slice in Fig. 1(c)]. A second phantom is also created that is identical except that the detailed $5 \times 5 \times 5$ cm^3 cube is filled with voxels of an averaged tissue with the same proportions by mass as the segmented detailed cube (26.4% fibroglandular and 73.6% adipose tissue). These phantoms are called "26.4/73.6-realistically-segmented phantom" and "26.4/73.6-averaged-tissue phantom," respectively, and the averaged tissue is denoted by "26.4/73.6-averaged-tissue." The position of the seeds and PTV remain the same as those of the randomly segmented phantom as they lie approximately in the center of the distribution of fibroglandular tissue.

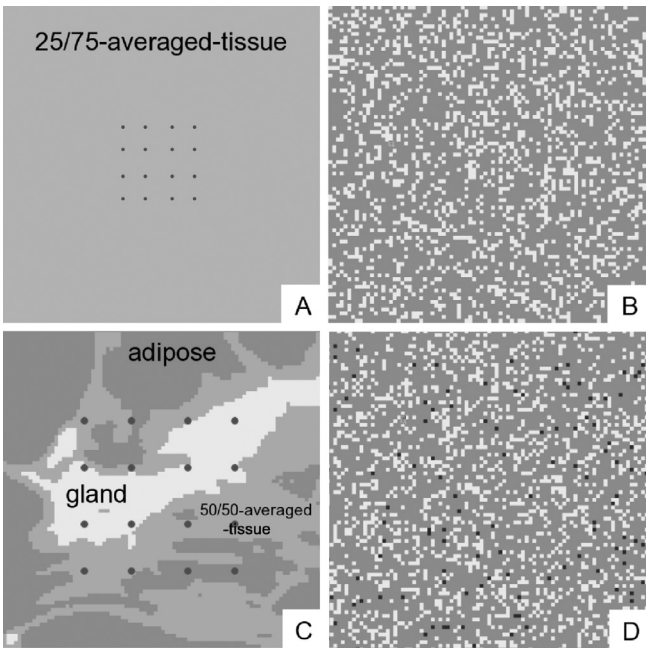

FIG. 1. Diagrams showing representational x-y slices of inner portions of various phantoms. (A) a slice in the 25/75-averaged-tissue phantom. (B) a slice of the 25/75-randomly-segmented phantom, (C) a representational slice of only the detailed inner section of the 26.4/73.6-realistically-segmented phantom and (D) a slice of the 22.5/72.5/5-randomly-segmented phantom. In (B) and (D), white/light gray represents gland voxels, gray represents adipose voxels, and black represents calcification. Seed positions are shown in dark gray in (A) and (C) but omitted in (B) and (D) for clarity. The seed positions in (B) and (D) would be the same as in (A).

To approximate the use of CT data to assign voxel densities, an additional modified averaged tissue phantom is created such that each voxel contains the averaged tissue material but with voxel densities identical to that of the realistically segmented phantom.

A second realistically segmented phantom is also created using another computational phantom from Zastrow *et al.* to confirm that the general trend of the results found are not dependent on the particular glandular density of the 26.5/73.6-realistically-segmented phantom. This denser phantom is composed of approximately 55% fibroglandular and 45% adipose tissues.

II.C. The effect of calcifications on photon energy fluence

A randomly segmented phantom is created composed of 22.5% fibroglandular tissue, 72.5% adipose tissue, and 5% calcification by mass (22.1%, 76.3%, and 1.6% by volume, respectively) with calcified (1 mm)^3 voxels distributed randomly throughout the entire phantom. The fraction of calcification was chosen based on results found in the literature.[22,23] While the dimensions of $1 \times 1 \times 1$ mm^3 used may be too small to represent the size of an average calcification, it serves well as a limiting case scenario; if small, randomly distributed calcifications significantly effect the ability to approximate the photon energy fluence with an averaged tissue, then larger ones will have an effect. This phantom is compared to an averaged tissue phantom of the same proportions, a second averaged tissue phantom where the density of each voxel matches that of the same voxel in the randomly segmented phantom, and a third averaged tissue phantom composed of 25% gland and 75% adipose with the same voxel densities as the randomly segmented phantom (that includes calcifications). The randomly segmented and averaged tissue phantoms are

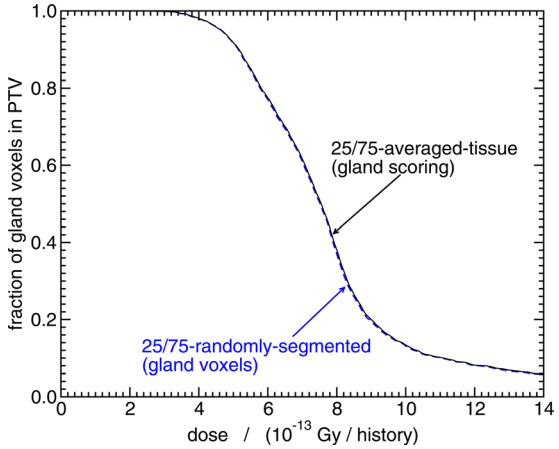

FIG. 2. The DVHs for the dose to fibroglandular tissue in phantoms of 25% fibroglandular tissue and 75% adipose tissue by mass. The DVH for a 25/75-randomly-segmented phantom where the volume considered consists only of those voxels that contain fibroglandular tissue is shown as well as the DVH for a 25/75-averaged-tissue phantom with dose scored in fibroglandular tissue where the volume considered is the same as that of the randomly segmented case.

denoted by "22.5/72.5/5-randomly-segmented phantom" and "22.5/72.5/5-averaged-tissue phantom," respectively, and the averaged tissue is denoted by 22.5/72.5/5-averaged-tissue. Figure 1(d) shows a representational slice of the 22.5/72.5/5-randomly-segmented phantom.

III. RESULTS AND DISCUSSION

III.A. Dose to gland and adipose versus dose to an averaged tissue

Figure 2 compares the DVHs for the dose to the gland voxels within the PTV of the 25/75-randomly-segmented phantom to the dose to the voxels corresponding to the same spatial coordinates of the 25/75-averaged-tissue phantom with dose scored in gland. The close agreement between the two curves implies that the media in the 25/75-randomly-segmented phantom is sufficiently uniformly distributed such that, to first order, the photon energy fluence remains the same between the two phantoms. This is confirmed by the fact that the explicitly calculated photon energy fluences at the center of each phantom agree within 2%. The agreement also implies that, in the very unlikely case that a realistic breast is also sufficiently uniform in its distribution of gland and adipose tissues (i.e., the photon energy fluence of a realistic breast remains unchanged from that of an averaged tissue phantom), the method used in mammography of photon transport in an averaged tissue and dose scoring in a fibroglandular tissue would provide accurate dose volume metrics and mean doses to glandular tissue.

Figure 3 compares the DVHs for the dose to the entire PTV for the 25/75-randomly-segmented phantom (dose to gland and adipose voxels) and 25/75-averaged-tissue phantom (with dose scored in 25/75-averaged-tissue) and illustrates that differences in the shape of the DVH can arise when an averaged tissue is used to approximate the dose scored to segmented gland and adipose voxels. A small but clear difference is present between the two curves (similar to the results of Afsharpour *et al.*[11]) which shows that, despite a nearly identical photon energy fluence for both calculations, inaccurate doses can occur when scoring in an averaged tissue.

The differences in shape between the two DVHs of Fig. 3 are explained by the differences in mass energy absorption coefficients (and will thus be sensitive to the choice of tissue composition). The mass energy absorption coefficient of gland is higher than that of 25/75-averaged-tissue and so, given the same photon energy fluence, those voxels containing gland will receive a higher dose and are seen in region A of the DVH. Conversely, adipose has a lower mass energy absorption coefficient than 25/75-averaged-tissue and so absorbed dose will be lower for the same photon energy fluence as seen in region B in the DVH. These effects are illustrated in Fig. 4, which shows a dose profile in the y-direction of the phantoms at $x = 0.2$ cm and $z = 0.2$ cm. The calculated

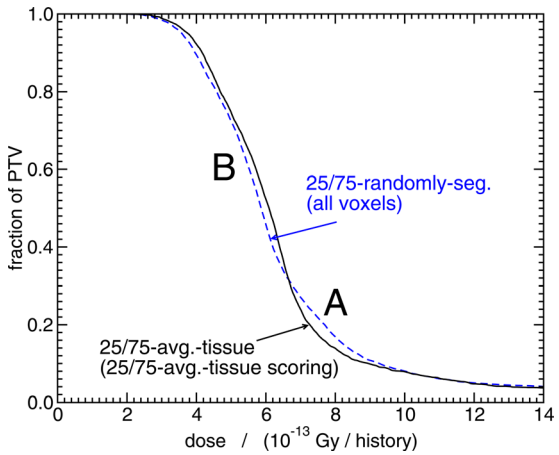

FIG. 3. DVHs for the entire PTV in phantoms of 25% fibroglandular tissue and 75% adipose tissue by mass. Shown is the DVH for a 25/75-randomly-segmented phantom where the volume considered is the entire PTV (both adipose and fibroglandular tissue voxels with the dose scored to individual materials) as well as the DVH for a 25/75-averaged-tissue phantom with dose scored in the 25/75-averaged-tissue, where the volume considered is also the entire PTV.

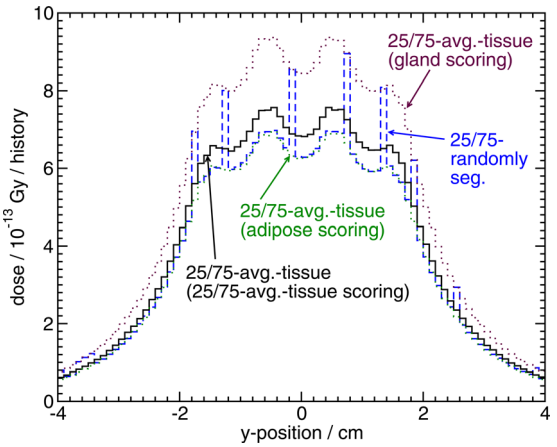

FIG. 4. Dose vs position along the y-direction ($x = 0.2$ cm and $z = 0.2$ cm) for a 25% fibroglandular and 75% adipose tissue mixture by mass. The doses for 25/75-randomly-segmented, 25/75-averaged-tissue (25/75-averaged-tissue scoring), 25/75-averaged-tissue (adipose scoring), and 25/75-averaged-tissue (gland scoring) calculations are shown.

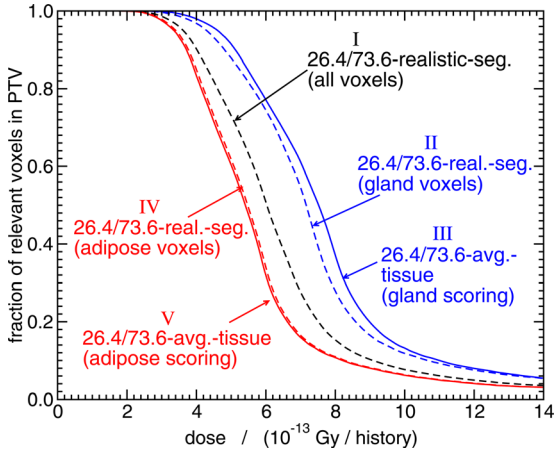

FIG. 5. The DVHs for the dose to fibroglandular, adipose or all tissues in phantoms of 26.4% fibroglandular tissue and 73.6% adipose tissue by mass. Curve I shows the dose to all voxels in a 26.4/73.6-realistically-segmented phantom. Curves II and III show the dose to the gland voxels in a 26.4/73.6-realistically-segmented phantom and the dose to those same voxels in a 26.4/73.6-averaged-tissue (gland scoring) phantom, respectively. Curves IV and V show the dose to the adipose voxels in a 26.4/73.6-realistically-segmented phantom and the dose to those same voxels in a 26.4/73.6-averaged-tissue (adipose scoring) phantom, respectively.

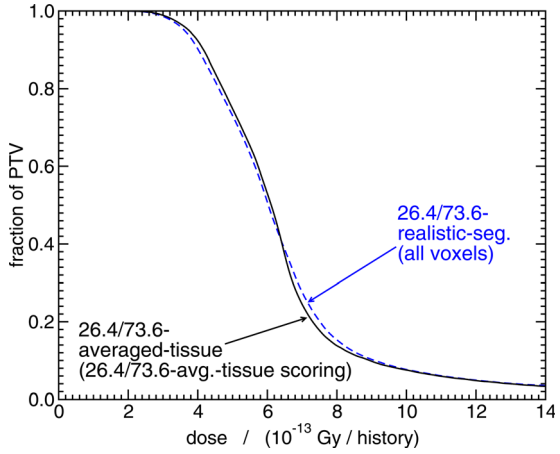

FIG. 6. The DVHs for the entire PTV in a realistically segmented (26.4/73.6) phantom of 26.4% fibroglandular tissue and 76.3% adipose tissue by mass (same proportions as in figure 5 and same as curve I in figure 5) and for a 26.4/73.6-averaged-tissue phantom of the same proportions of tissue by mass with dose scored in the 26.4/73.6-averaged-tissue.

dose in the 25/75-randomly-segmented phantom is higher or lower than that in the 25/75-averaged-tissue (25/75-averaged-tissue scoring) calculation depending on whether the voxel being considered is fibroglandular or adipose tissue. The 25/75-averaged-tissue (gland scoring) and 25/75-averaged-tissue (adipose scoring) results show agreement on the order of 0.5%–1% with the 25/75-randomly-segmented phantom when the voxel being considered is fibroglandular tissue or adipose tissue, respectively, which again is a result of the similar photon energy fluences in both phantoms.

III.B. Realistic segmentation and its effect on photon energy fluence

Curves II and III in Fig. 5 compare the DVHs for the dose to only the gland voxels within the PTV of the 26.4/73.6-realistically-segmented phantom (curve II) to the dose to the voxels corresponding to the same spatial coordinates of the 26.4/73.6-averaged-tissue phantom with dose scored in gland (curve III). It was observed in Fig. 2 that gland scoring resulted in DVHs having unnoticeable difference between the 25/75-randomly-segmented and 25/75-averaged-tissue phantoms because on average the photon energy fluences were very close to each other. In Fig. 5, however, the lower gland dose in the 26.4/73.6-realistically-segmented phantom implies that the photon energy fluence within the fibroglandular tissue voxels is lower on average than in those of same voxels in the 26.4/73.6-averaged-tissue phantom. This is explained by the fact that a phantom with realistic segmentation has larger groupings of fibroglandular tissue voxels. The voxels toward the center of these groupings are surrounded by other fibroglandular tissue voxels, and photons delivering dose in these voxels will have experienced more attenuation compared to photons in the same voxels of an averaged tissue phantom as a result of the higher density and mass attenuation coefficient of gland. Hence, the dose is lower in these voxels due to reduced photon energy fluence.

Curve I in Fig. 5 shows the DVH for the 26.4/73.6-realistically-segmented phantom, where all the voxels are considered, and the dose is scored in the local medium. The large difference between curve I and the one for only the gland voxels (II) illustrates the need to treat each tissue individually if the dose to a single tissue is of interest.

Curves IV and V in Fig. 5 compare the DVHs for the dose to only the adipose voxels within the PTV of the 26.4/73.6-realistically-segmented phantom (IV) to the dose to the same voxels of the 26.4/73.6-averaged-tissue phantom with dose scored in adipose (V). The larger groupings of adipose tissue (compared to a randomly segmented phantom) will cause the photon energy fluence in those voxels to be higher in a realistically segmented phantom than in the same voxels in an averaged tissue phantom. However, as the averaged tissue is 73.6% adipose by mass, the differences in photon energy fluence in the adipose tissue groupings will be less dramatic than in the case of gland tissue. This is reflected in the close agreement between curves IV and V.

Figure 6 compares the DVHs for the dose to the entire PTV for the 26.4/73.6-realistically-segmented phantom with the dose scored in each medium and the 26.4/73.6-averaged-tissue phantom (with dose scored in 26.4/73.6-averaged-tissue). While the differences between the DVHs are qualitatively similar to those of Fig. 3, they are smaller in magnitude. In this case, the change in photon energy fluence implied by Fig. 5 compensates to some degree for the change in scored dose as a result of scoring in gland and adipose versus averaged tissue (regions A and B in Fig. 3). These competing effects combine to produce a calculation that provides more accurate dose volume histograms when considering the DVH for all PTV voxels.

Additionally, the differences seen in the comparison of curves II and III in Fig. 5 reflect the inaccuracy of using the photon energy fluence in an averaged tissue to approximate the photon energy fluence in the gland voxels of a

realistically segmented phantom. The gland voxels in a realistically segmented phantom will have a lower photon energy fluence on average than the same voxels of an averaged tissue phantom. This result is somewhat ameliorated in the comparison of the DVHs in Fig. 6 (where all voxels are considered) because considering both gland and adipose voxels of a realistically segmented phantom will mean that lower photon energy fluence in gland and higher photon energy fluence in adipose will both be included in the same volume. While photon energy fluence may differ significantly on a voxel by voxel basis, the *average* photon energy fluence in the entire PTV for an averaged tissue phantom will be closer to the average photon energy fluence in realistically segmented gland and adipose voxels than it will to the photon energy fluence in gland voxels alone. This will be reflected as increased agreement in dose volume histograms.

In general, an averaged tissue phantom with individual voxel densities equal to that of a realistically segmented phantom will have a photon energy fluence in closer agreement with that of the realistically segmented phantom. However, as the densities of gland and adipose differ to a much smaller degree than the mass attenuation coefficients (approximately 7% vs 20% difference, respectively), the modeling of voxels of varying density does not fully overcome the differences in photon energy fluence. For example, in Fig. 5, the difference between the minimum dose that 90% of the volume receives (D90) for the 26.4/73.6-realistically-segmented (gland voxels) calculation and the 26.4/73.6-averaged-tissue (gland scoring) calculation is approximately 6.3%. The use of a 26.4/73.6-averaged-tissue phantom with voxel densities equal to that of the 26.4/73.6-realistically-segmented phantom (not shown) only reduces the difference to 4.9%.

It is important to note that the improvement in dose volume metrics that would result from improved simulation of photon energy fluence would only occur if one was considering the dose to either gland or adipose. The inaccuracy of using an averaged tissue phantom when the dose to gland is desired results from inaccurate photon energy fluence alone and so any improvement in photon energy fluence will lead to improvement in dose volume metrics. In contrast, for dose to an entire volume (both gland and adipose), what accuracy exists in DVHs (Fig. 6) is a result of the competing effects of inaccurate photon energy fluence and inaccuracies from dose scored in averaged tissue rather than gland and adipose (regions A and B in Fig. 3). Consequently, an improvement in photon energy fluence simulation will nullify the competing effect and the differences shown in Fig. 3 will resurface.

A second realistically segmented phantom was created using another computational phantom from Zastrow *et al.*[21] This phantom was composed of approximately 55% fibroglandular and 45% adipose tissues. The effects found in Figs. 5 and 6 were qualitatively identical but with slightly differing magnitude with this denser phantom. This confirms that the results of this work are not unique to the particular glandular density in the phantom used.

The results from the simulations with a seed configuration approximating a small, dense treatment (not presented) confirm the general effects and their relative magnitudes discussed above.

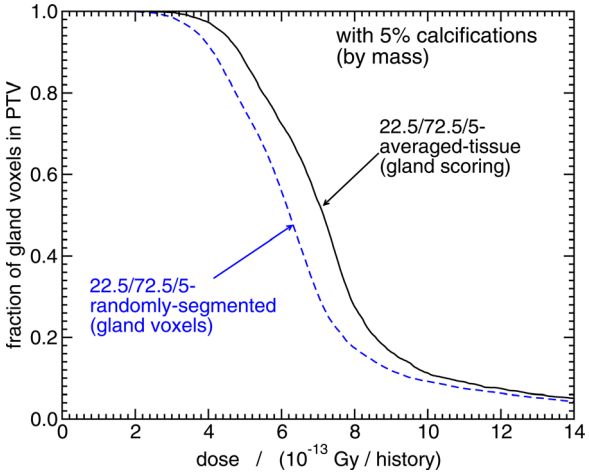

FIG. 7. DVHs for phantoms composed of 22.5% fibroglandular tissue, 72.5% adipose tissue, and 5% calcification by mass. Shown are the DVH calculated from a 22.5/72.5/5-randomly-segmented phantom (with (1 mm)^3 calcifications) considering only those voxels containing fibroglandular tissue as well as the DVH from a 22.5/72.5/5-averaged-tissue (gland scoring) phantom with the same voxels considered as the 22.5/72.5/5-randomly-segmented phantom.

In all calculations, the choice of tissue compositions can significantly affect the dose calculated in the breast. For instance, the compositions in Hammerstein *et al.*[3] could be used instead of those of Woodard and White and this choice would affect the magnitude of the effects discussed in this work (e.g., the mass energy absorption coefficient for gland at 20 keV is 17% lower for the composition in Woodard and White than that in Hammerstein *et al.*) but would not change the conclusions.

III.C. The effect of calcifications on photon energy fluence

A 22.5/72.5/5-randomly-segmented phantom with 22.5% fibroglandular tissue, 72.5% adipose tissue, and 5% calcification by mass was created. In Fig. 7, the DVH for the dose to the fibroglandular voxels within the PTV is compared to the DVH of the voxels corresponding to the same spatial coordinates for a 22.5/72.5/5-averaged-tissue phantom (gland scoring). The lower dose for the 22.5/72.5/5-randomly-segmented phantom shows that, despite the media being randomly distributed, calcifications in the breast significantly lower the average photon energy fluence.

Figure 8 contains DVHs calculated for the entire PTV. Curve I shows the DVH for the entire PTV for the 22.5/72.5/5-randomly-segmented phantom. The disagreement between curve I and the DVH for the 22.5/72.5/5-averaged-tissue phantom with dose scored in 22.5/72.5/5-averaged-tissue (curve II) shows that the difference in photon energy fluence between the 22.5/72.5/5-randomly-segmented phantom and the 22.5/72.5/5-averaged-tissue phantom is too large to be compensated for by changes in scored dose between gland, adipose, calcification, and the 22.5/72.5/5-averaged-tissue of those three media. Curve III

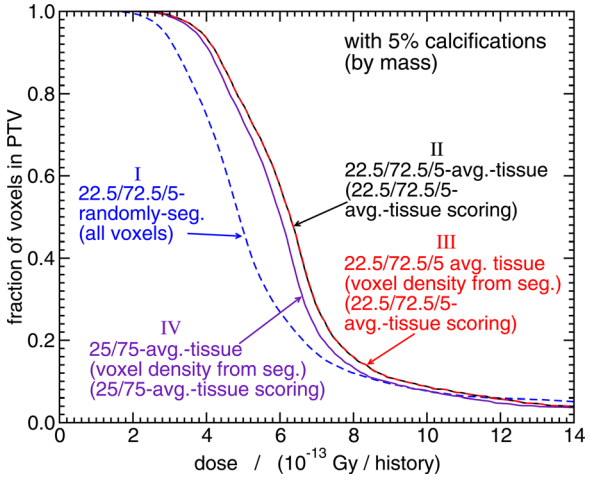

FIG. 8. DVHs for phantoms composed of 22.5% fibroglandular tissue, 72.5% adipose tissue, and 5% calcification by mass. In all cases, DVHs are calculated considering all voxels in the PTV. Shown are the DVH calculated from a 22.5/72.5/5-randomly-segmented phantom (with (1 mm)^3 calcifications) considering every voxel within the PTV (I), the DVH from a 22.5/72.5/5-averaged-tissue (22.5/72.5/5-averaged-tissue scoring) phantom of a single averaged density (II), the DVH from a 22.5/72.5/5-averaged-tissue) (22.5/72.5/5-averaged-tissue scoring) phantom where voxel densities match those of the 22.5/72.5/5-randomly-segmented phantom (III), and a 25/75-averaged-tissue (25/75-averaged-tissue scoring) phantom where voxel densities are identical to those of curves I and III (IV).

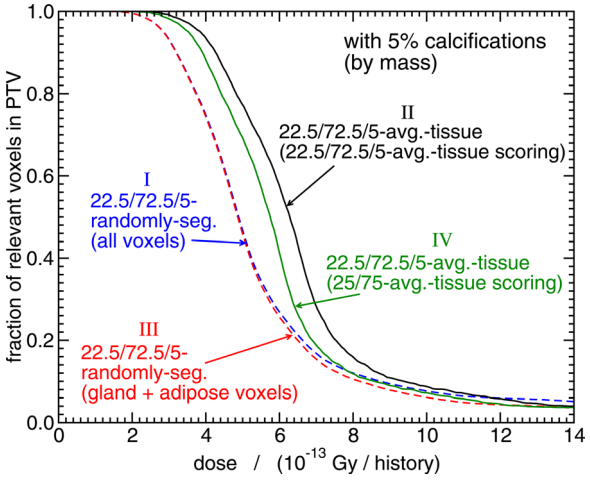

FIG. 9. DVHs for phantoms composed of 22.5% fibroglandular tissue, 72.5% adipose tissue, and 5% calcification by mass. Curves I and II show the DVHs for all the voxels in the PTV for the 22.5/72.5/5-randomly-segmented phantom and 22.5/72.5/5-averaged-tissue (22.5/72.5/5-averaged-tissue scoring) phantom, respectively. Curve III is the DVH for the gland and adipose voxels of the 22.5/72.5/5-randomly-segmented phantom, and curve IV is the DVH for the 22.5/72.5/5-averaged-tissue (25/75-averaged-tissue scoring) phantom.

is for calculations with a phantom that contains a 22.5/72.5/5-averaged-tissue of gland, adipose, and calcification but with the density of each voxel assigned to the density of the same voxel in the randomly segmented phantom. The fact that curve III closely agrees with curve II implies that the assignment of accurate voxel densities does not improve the ability of an averaged tissue phantom to approximate the photon energy fluence of a segmented phantom when calcifications are present. The inaccuracy in the photon energy fluence must result almost entirely from the inability of an averaged tissue to model the significant difference between the mass attenuation coefficients of gland and adipose versus calcifications.

Curve IV of Fig. 8 shows the DVH calculated for a phantom containing a 25/75-averaged-tissue composed of only gland and adipose, where voxel densities are assigned to the density of the same voxel in the 22.5/72.5/5-randomly-segmented phantom (curve I) (i.e., some voxels will have the density of calcification). This curve is used to approximate the result one would achieve if the presence of calcifications was not considered in the material composition of the breast, but the density of the calcifications was taken from CT data. Although curve IV significantly disagrees with the randomly segmented model, it is slightly closer than curves II and III. This shift to the left results from the decrease in mass energy absorption coefficient for 25/75-averaged-tissue when the calcifications are not included.

Figure 9 illustrates the effect of considering the dose to only the gland and adipose in a phantom that contains calcifications. Curves I and II are identical to curves I and II of Fig. 8. Curve III shows the DVH for only the gland and adipose voxels of the 22.5/72.5/5-randomly-segmented phantom. As the voxels containing calcification only correspond to 1.6% of total volume, the omission of the dose to the calcifications has a little effect on the DVH. This differs from curve IV, which shows the DVH (for the same voxels as those considered for curve III) of a 22.5/72.5/5-averaged-tissue (25/75-averaged-tissue scoring) phantom. In this calculation, photon transport occurs in an averaged tissue containing calcification but dose delivery in an averaged tissue without calcification. While the elimination of calcification (and its high Z contribution to composition) from the scoring averaged tissue moves curve IV closer to agreement with curve III (compared with II versus I), the inability of the 22.5/72.5/5-averaged-tissue phantom to approximate the photon energy fluence of the 22.5/72.5/5-randomly-segmented phantom is clear.

IV. CONCLUSIONS

The photon energy fluence is not accurately determined if an averaged tissue phantom is used in Monte Carlo simulations. Given the typical composition of the breast,[2] if the dose to gland tissue within the volume considered is desired, then the phantom must be properly segmented to achieve accurate doses and dose volume metrics. If dose to adipose tissue is desired, then an averaged tissue (adipose scoring) phantom may be sufficient to achieve accurate dose volume metrics. If dose metrics for the entire volume (all tissues) are desired, and the dose is scored in an averaged tissue, inaccuracies in the photon energy fluence will partially compensate for inaccuracies in scoring dose in an averaged tissue rather than in gland and adipose separately. While significant dose differences may exist on a voxel by voxel basis, reasonably correct dose volume metrics will result.

Regardless of whether the dose to a single tissue or an entire volume is desired, the consideration of calcifications

in a breast phantom necessitates the use of realistic segmentation as the effect of the composition of calcifications on the photon energy fluence is large.

Further work is required to extend the conclusions of the current work for ^{103}Pd to other low-energy brachytherapy sources (e.g., ^{125}I and 50 kV electronic brachytherapy sources). While the ratio of mass energy absorption coefficients of gland to adipose remain relatively constant in the energy range of interest, the ratio of mass attenuation coefficients of gland to adipose converges as energy increases, reaching approximately 1.05 at 50 keV. It is expected that the observed effects are not as important for higher-energy sources such as ^{192}Ir, because the mass energy absorption and mass attenuation coefficients of the breast tissues are in much closer agreement at these photon energies.

The assignment of voxel densities based on CT data to an averaged tissue phantom reduces differences seen in photon energy fluence but not to such a degree that differences in dose volume metrics disappear.

It is likely that the methods commonly used in mammography radiation protection calculations overestimate the average dose to the glandular tissue. This arises because the averaged tissue phantoms do not accurately reflect the photon energy fluence in the gland of a realistic breast.

ACKNOWLEDGMENTS

J. G. H. Sutherland is supported by an OGSST scholarship, and the work is supported by NSERC, the CRC program, CFI, OIT, MRIO ,and the office of the Vice-President of Research at Carleton University. E. S. M. Ali and B. Muir are thanked for their useful comments on the manuscript.

[a]Author to whom correspondence should be addressed. Electronic mail: jsutherl@physics.carleton.ca

[1]M. J. Rivard *et al.*, "Update of AAPM Task Group No. 43 Report: A revised AAPM protocol for brachytherapy dose calculations," Med. Phys. **31**, 633–674 (2004).
[2]M. J. Yaffe *et al.*, "The myth of the 50-50 breast," Med. Phys. **36**, 5437–5443 (2009).
[3]G. R. Hammerstein, D. W. Miller, D. R. White, M. E. Masterson, H. Q. Woodard, and J. S. Laughlin, "Absorbed radiation dose in mammography," Radiology **130**, 485–491 (1979).
[4]D. R. Dance, "The Monte Carlo calculation of integral radiation dose in xeromammogrpahy," **25**, 25–37 (1980).
[5]I. Sechopoulos, A. Karellas, S. Suryanarayanan, S. Vedantham, and C. D'Orsi, "Computation of the glandular radiation dose in digital tomosynthesis of the breast," Med. Phys. **34**, 221–232 (2007).
[6]R. C. Chen *et al.*, "Measurement of the linear attenuation coefficients of breast tissues by synchrotron radiation computed tomography," Phys. Med. Biol. **55**, 4993–5005 (2010).
[7]P. C. Johns and M. J. Yaffe, "X-ray characterisation of normal and neoplastic breast tissues," Phys. Med. Biol. **32**, 675–696 (1987).
[8]H. Afsharpour, J.-P. Pignol, B. Keller, J.-F. Carrier, B. Reniers, F. Verhaegen, and L. Beaulieu, "Influence of breast composition and interseed attenuation in dose calculations for post-implant assessment of permanent breast 103 Pd seed implant," Phys. Med. Biol. **55**, 4547–4561 (2010).
[9]G. Landry *et al.*, "Sensitivity of low energy brachytherapy Monte Carlo dose calculations to uncertainties in human tissue composition," Med. Phys. **37**, 5188–5198 (2010).
[10]C. Furstoss *et al.*, "Monte Carlo study of LDR seed dosimetry with an application in a clinical brachytherapy breast implant, Med. Phys. **36**, 1848–1858 (2009).
[11]H. Afsharpour, J.-P. Pignol, B. Keller, J.-F. Carrier, B. Reniers, F. Verhaegen, and L. Beaulieu, "Toward a more accurate dose calculation technique using a semiautomatic organ contouring in Monte Carlo post-implant assessment of breast LDR brachytherapy," Abstract book of MCTP2009: Second European Workshop on Monte Carlo Treatment Planning, pp. 98–101 (2009), available at www.mctp2009.org/images/documents/EGW-MCTP%20Workshop%202009%20Book%20of%20Abstracts.pdf.
[12]M. Bazalova and E. E. Graves, "The importance of tissue segmentation for dose calculations for kilovoltage radiation therapy," Med. Phys. **38**, 3039–3049 (2011).
[13]I. Kawrakow and D. W. O. Rogers, The EGSnrc Code System: Monte Carlo simulation of electron and photon transport, NRC Technical Report No. PIRS-701 v4-2-2-5, National Research Council of Canada, Ottawa, Canada. http://www.irs.inms.nrc.ca/inms/irs/EGSnrc/EGSnrc.html, 2007.
[14]R. E. P. Taylor, G. Yegin, and D. W. O. Rogers, "Benchmarking BrachyDose: voxel-based EGSnrc Monte Carlo calculations of TG–43 dosimetry parameters," Med. Phys. **34**, 445–457 (2007).
[15]R. M. Thomson, G. Yegin, R. E. P. Taylor, J. G. H. Sutherland, and D. W. O. Rogers, "Fast Monte Carlo Dose calculations for Brachytherapy with BrachyDose," Med. Phys. **37**, (abstract) 3910–3911 (2010).
[16]R. E. P. Taylor and D. W. O. Rogers, "An EGSnrc Monte Carlo-calculated database of TG-43 parameters," Med. Phys. **35**, 4228–4241 (2008).
[17]R. M. Thomson and D. W. O. Rogers, "Monte Carlo dosimetry for ^{125}I and ^{103}Pd eye plaque brachytherapy with various seed models," Med. Phys. **37**, 368–376 (2010).
[18]J.-P. Pignol, E. Rakovitch, B. M. Keller, R. Sankreacha, and C. Chartier, "Tolerance and Acceptance Results of a Palladium-103 Permanent Breast Seed Implant Phase I/II Study," Int. J. Radiat. Oncol. Biol. Phys. **73**, 1482–1488 (2009).
[19]H. Q. Woodard and D. R. White, "The composition of body tissues," Brit. J. Radiol. **59**, 1209–1219 (1986).
[20]Photon, Electron, Photon and Neutron Interaction Data for Body Tissues, ICRU Report No. 46 (ICRU, Washington, DC, 1992).
[21]E. Zastrow, S. K. Davis, M. Lazebnik, F. Kelcz, B. D. V. Veen, and S. C. Hagness, "Development of anatomically realistic numerical breast phantoms with accurate dielectric properties for modeling microwave interactions with the human breast," IEEE Trans. Biomed. Eng. **55**, 2792–2800 (2010).
[22]O. Hassler, "Microradiographic investigations of calcifications of the female breast," Cancer **23**, 1103–1109 (1969).
[23]D. M. Hansell, J. C. Cooke, C. A. Parsons, S. H. Evans, D. R. Dance, J. M. Bliss, and I. Ilesley, "A quantitative analysis of the spatial relationships of grouped microcalcifications demonstreated on xeromammography in benign and malignant breast disease," Brit. J. Radiol. **61**, 21–25 (1988).